Hydrothermally Synthesized CeO_2 Nanowires for H_2S Sensing at Room Temperature

Zhijie Li[1], Xinyue Niu[1], Zhijie Lin[1], Ningning Wang[1], Huahai Shen[1], Wei Liu[1], Kai Sun[2], Yong Qing Fu[1,3*], Zhiguo Wang[1*]

[1]School of Physical Electronics, University of Electronic Science and Technology of China, Chengdu 610054, PR China
[2]Department of Nuclear Engineering and Radiological Sciences, University of Michigan, Ann Arbor, MI 48109-2104, USA
[3]Department of Physics and Electrical Engineering, Faculty of Engineering and Environment, Northumbria University, Newcastle Upon Tyne NE1 8ST, United Kingdom

Abstract

CeO_2 nanowires were synthesized using a facile hydrothermal process without any surfactant, and their morphological, structural and gas sensing properties were systematically investigated. The CeO_2 nanowires with an average diameter of 12.5 nm had a face-centered cubic fluorite structure and grew along [111] of CeO_2. At the room temperature of 25 ^oC, hydrogen sulfide (H_2S) gas sensor based on the CeO_2 nanowires showed excellent sensitivity, low detection limit (50 ppb), and short response and recovery time (24 s and 15 s for 50 ppb H_2S, respectively).

Keywords: CeO_2, Nanowires, Hydrothermal, Sensitivity, Gas sensor

* Corresponding author. Tel.: +86 02883200728. E-mail address: zgwang@uestc.edu.cn (Zhiguo Wang); Richard.fu@northumbria.ac.uk (Yong Qing Fu)

1 Introduction

Cerium oxide (CeO_2) based nano-material, one of multi-functional n-type semiconductor materials, have attracted great attention recently because of its superior catalytic performance [1-5], optical properties [6-8], oxygen storage capacity [9], and magnetic properties [10-12]. Therefore, it has been widely used in the field of catalyst [1-3], photocatalyst [4-5], solid oxide fuel cells [6-7], oxygen pump [9] and luminescence materials [13-15]. Recently, CeO_2 has also been proposed for one potential sensing material in the field of solid state gas sensors for environmental monitoring, such as CO [16,17], CH_4 [17], O_2 [18], NO_2 [19], carbon disulfide [20] and humidity [21]. Nanostructured CeO_2 could significantly enhance the gas sensing performance because of its characteristic structural and electronic properties as mentioned above. It is generally accepted that increasing surface area to volume ratio and decreasing crystal sizes of the CeO_2 are crucial to achieve a highly sensitive gas sensors [21]. Apart from crystal size, different crystal structures and surface morphologies of the CeO_2 nanomaterials could affect their physical and chemical properties and provide new functions for applications. Recently, one-dimensional (1D) CeO_2 nanostructures have attracted great attention. Much effort has been made on the fabrication of 1D CeO_2 nanowires using electrochemical assembly [6,22], electro-spinning [23], precipitation [24-25], and hydrothermal method [4,26-30]. Compared with other preparation methods to synthesize the CeO_2 nanostructures, hydrothermal methods have advantages of low synthesis temperature and no need for post-sintering. Most of the current synthesis approaches to grow the hierarchical

architectures (including 1D nanostructure) require templates or surfactants, or complicated procedures [27-28]. It remains a challenge to develop facile and effective template-free methods for 1-D CeO_2 nanostructures with various properties and applications. The gas sensor based on the 1-D CeO_2 nanostructures to detect the H_2S has never been reported.

This paper reported a hydrothermal process to prepare CeO_2 nanowires without using any template or surfactant. The gas sensor for detecting H_2S at room temperature was fabricated and characterized using the CeO_2 nanowires.

2. Experimental procedures

2.1 Synthesis and characterization

$Ce(NO_3)_3 \cdot 9H_2O$, urea and NaOH of analytical grade were purchased from Sinopharm Chemical Reagents Co., Ltd (Shanghai, China) and used as received without any further purification. De-ionized water with a resistivity of 18.0 MΩ·cm was used throughout the synthesis process. The CeO_2 nanowires were synthesized using a hydrothermal reaction method. In a typical synthesis process, a mixed solution was prepared by dissolving NaOH (40.0 g) and urea (15.0 g) into 100 ml deionized water. Then, 10 ml $Ce(NO_3)_3 \cdot 6H_2O$ solution (0.5 mol/L) was slowly dripped into the mixed solution under continuously stirring to form a suspension. The suspension was stirred for 30 minutes and then transferred into a 150 mL Teflon-lined stainless steel autoclave for a hydrothermal reaction at 100 °C for 24 hours. After that, the product was cooled down to room temperature, centrifuged, washed with deionized water and anhydrous ethanol for three times. Finally, it was dried in air at 70 °C for 10 hours to

obtain the CeO_2.

Crystalline phases of the CeO_2 nanowires were determined using X-ray diffraction (XRD, CuKα, 40kV, 60mA, Rigaku D/max-2400). The morphologies were observed using scanning electron microscopy (SEM, Inspect F50, USA). High resolution transmission electron microscope (HRTEM, JEM-2200FS, Japan) was used to characterize crystallographic features of the sample. The specific BET (Brunner−Emmet−Teller) surface areas of the CeO_2 nanostructures were measured using nitrogen adsorption isotherm at 77 K (Tristar3000, Micromeritics). The chemical state of CeO_2 nanostructures was determined using a KRATOS XSAM 800 X-ray photoelectron spectrometer (XPS) with monochromatic AlKα (hv = 1486 eV) radiation. Diffuse reflectance spectrum (DRS) was recorded using a Shimadzu UV-2101 apparatus, equipped with an integrating sphere, using $BaSO_4$ as the reference.

2.2 Gas sensor fabrication and measurement

Gas-sensing performance of the device was evaluated using a WS-30A gas sensor measurement system (Weisen Electronic Technology Co., Ltd., Zhengzhou, China) at the room temperature of 25 ^oC. Fabrication processes of the gas sensor are as follows: (i) the as-prepared CeO_2 nanowires were mixed with absolute ethyl alcohol with a weight ratio of 1:4 and then ultrasonically agitated for 15 min until the formation of a homogeneous slurry; (ii) the slurry was pasted onto an alumina tube; (iii) the CeO_2 coated alumina tube was calcined at 300 ^oC for 2 hours to improve the stability of the sensor and remove the residual organics on the surface of sensor. Fig. 1a shows the

schematic illustration of the gas sensor, where a Ni-Cr heater was placed inside the alumina tube as a resistor to control the working temperature of the sensor. A pair of gold electrodes were connected onto the alumina tube, and two Pt wires have been used to form measurement circuit for resistance measurements. Fig. 1b displays a measurement circuit of the gas sensor, where R_E is a load resistor connected in series with the gas sensor, and R_S donates the resistor of the sensor. During sensing testing, an appropriate working voltage (Vs=5 V) was applied and the response of the sensor was monitored from the voltage changes of the R_E. The gas response (S) is defined as: $S=R_a/R_g$, where the R_a and R_g are the resistances values from the sensor measured in air and the target H_2S gas, respectively.

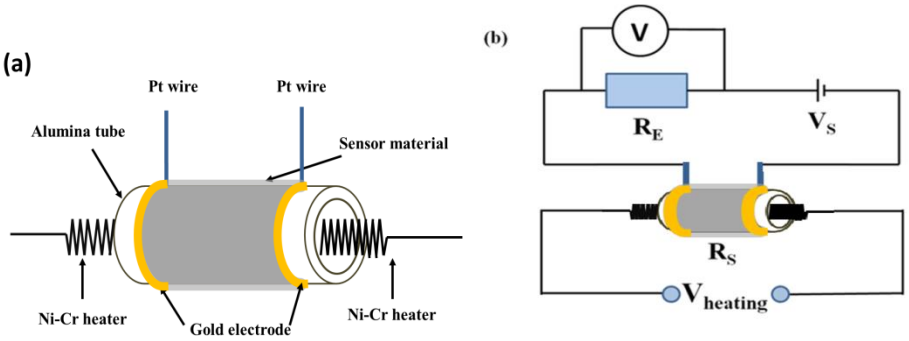

Fig.1 (a) Schematic of the gas sensor based on CeO_2 nanowires sensing materials, (b) The measurement electric circuit for the gas sensor.

3. Results and discussion

3.1 Structural and morphological characteristics

Fig. 2 shows the XRD spectrum of the as-prepared CeO_2 nanowires sample. The characteristic diffraction peaks corresponded to the (111), (200), (220), (311), (222), (400), (311) and (420) planes of a face-centered cubic fluorite structure of CeO_2 (with

a lattice constant of a = 0.5411 nm according to JCPDS file 34-0394). No obvious peaks corresponding to cerium nitrate or other types of cerium oxides were identified from the XRD results, indicating that the sample is pure CeO_2.

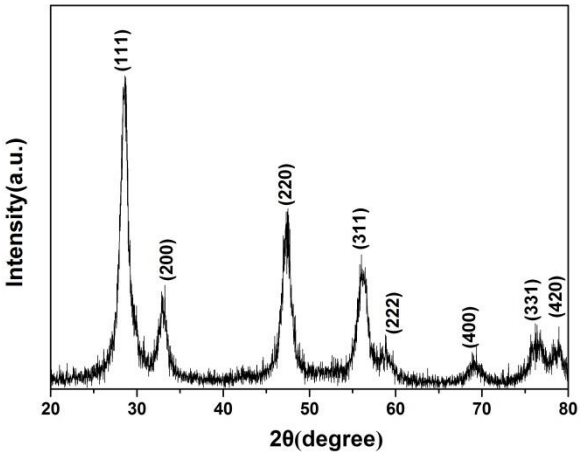

Fig. 2 XRD spectrum of CeO_2 nanowires

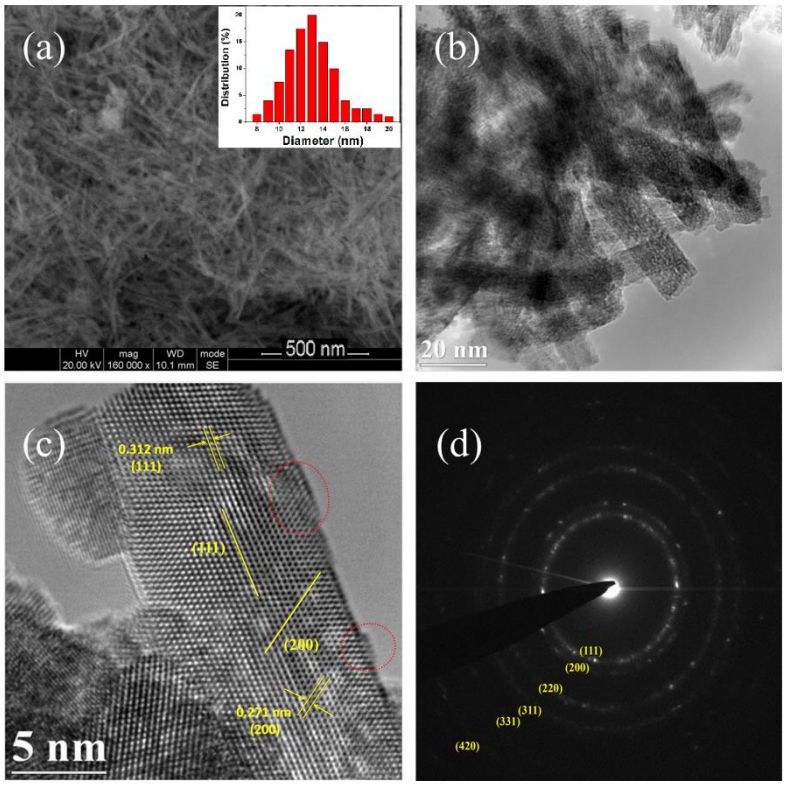

Fig. 3 (a) SEM image (inset indicates the size distribution histogram of diameter of nanowires), (b) TEM image, (c) HRTEM image and (d) the selected area electron diffraction pattern (SAED) of the obtained CeO_2 sample.

Fig. 3a and Fig 3b display the SEM and TEM images of the obtained CeO_2 sample, respectively. A large quantity of nanowires with an average diameter of 12.5 nm are clearly seen, and there are also a small amount of nanoparticles with an average diameter of about 8.0 nm. Fig. 3c shows the HRTEM image of the individual CeO_2 nanowires, revealing that they are structurally uniform and single crystalline in nature. The growth direction of the CeO_2 nanowires is along [111]. The lattice fringes in Fig. 3c illustrate two interplanar spacing values, i.e., 0.312 and 0.271 nm, which are consistent with the (111) and (200) planes of the CeO_2, respectively. There are some defects on the surface of CeO_2 nanowires (see the area in red circle), which could provide more reaction centers for the gas sensing. The crystalline nature of the resultant CeO_2 nanowires could be verified by the selected area electron diffraction (SAED) pattern (Fig. 3d) which is basically a ring pattern. The diffraction rings in the pattern can be indexed to (111), (200), (220), (311), (331) and (420) planes of the crystalline face-centered cubic structure, which is consistent with the XRD spectrum.

It is well-known that the Ce(III) oxidation state is unstable compared with the Ce(IV) oxidation state in alkaline solution [31]. In the experiment, Ce^{3+} oxidation state resulted in the formation of hydrated Ce^{4+} oxide as shown below:

$$4Ce^{3+} + 12\ OH^- + O_2 + (4n-6)H_2O \rightarrow 4(CeO_2 \cdot nH_2O) \quad (1)$$

In the hydrothermal process, urea could yield NH_3 and CO_2 through controlled hydrolysis in aqueous solutions (Equation (2)), i.e.:

$$CO(NH_2)_2 + H_2O \rightarrow CO_2 + 2NH_3 \quad (2)$$

It is clear that the NH_3 played an important role for nanowire growth. After the initial nucleation, the monomers would grow into $CeO_2 \cdot H_2O$ nanoparticles, and the NH_3 gas bubbles would be absorbed on its surface. In the present reaction system, microbubbles of NH_3 provided a bridge-linking role for the aggregation of these nanoparticles. Nanoparticles might aggregate around the gas–liquid interfaces between the NH_3 and water to form $CeO_2 \cdot H_2O$ nanowires. With the prolonging of the hydrothermal reaction, the $CeO_2 \cdot H_2O$ was crystallized and transformed into CeO_2 at an elevated temperature of 100 ^oC, i.e.:

$$CeO_2 \cdot nH_2O \rightarrow CeO_2 + nH_2O \quad (3)$$

Using the analysis from the BET surface area, the obtained specific surface area of the as-deposited CeO_2 nanowires were 86.0 $m^2 \cdot g^{-1}$. The nano-size diameters and large surface areas of CeO_2 nanowires are suitable for gas sensing.

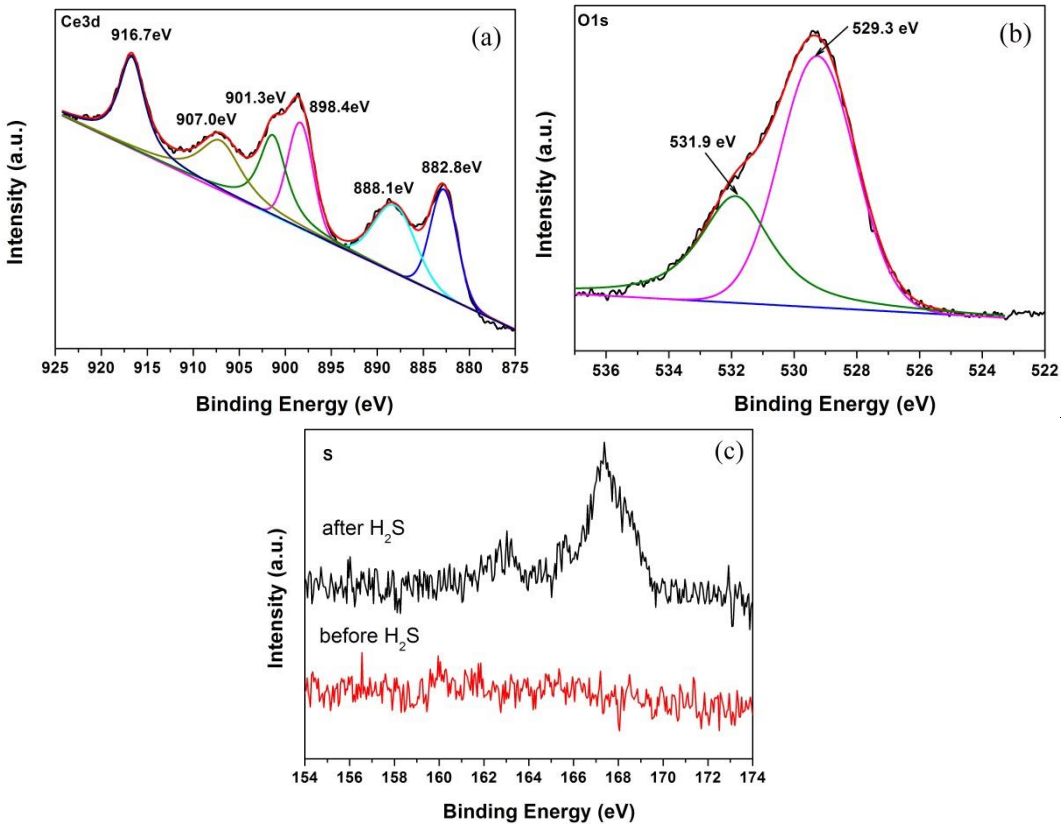

Fig. 4 XPS spectra of CeO_2 nanowires: (a) Ce 3d, (b) O 1s, (c) S before and after exposure to H_2S.

Fig. 4 shows the Ce 3d and O 1s XPS spectra of the CeO_2 nanowires. The Ce 3d spectrum (see Fig. 4a) shows six peaks resulting from three pairs of spin–orbit splits with different state configurations of $4f^i$ (i = 0, 1, 2). The peaks located at around 882.8 eV, 888.1 eV and 898.4 eV are assigned to the Ce $3d_{5/2}$, and those at around 901.3 eV, 907.0 eV and 916.7 eV are assigned to the Ce $3d_{3/2}$. The high binding energy of 916.9 eV and 898.4 eV are assigned to the final state of Ce(IV) $3d^9 4f^0$ $O2p^6$. The peaks at 907.5 eV and 888.9 eV are assigned to the hybridization state of Ce(IV) $3d^9 4f^1$ $O2p^5$, and those at 901.0 eV and 882.3 eV assigned to the state of Ce(IV) $3d^9 4f^2$ $O2p^4$ [32, 33]. It is obvious that the samples are in the state of Ce^{4+} without any impurity of the Ce^{3+} state. The XPS O 1s spectrum (Fig. 4b) is asymmetric and deconvoluted into 529.3 eV and 531.9 eV, respectively. The peak at 529.3 eV is assigned to the oxygen located in the CeO_2 crystal lattice [33], and that at around 531.9 eV is assigned to hydroxyl groups on the surface of CeO_2. Clearly there are large numbers of hydroxyl groups on the CeO_2 surface according to the high peak intensity, which might result in a high electrochemical activity. Fig. 4c shows the XPS spectra of CeO_2 nanowires before and after exposure to 100 ppm H_2S gas. It can be seen that a signal of S element appeared after it was exposed to H_2S, indicating that the adsorption of H_2S on the surface of CeO_2 nanowires.

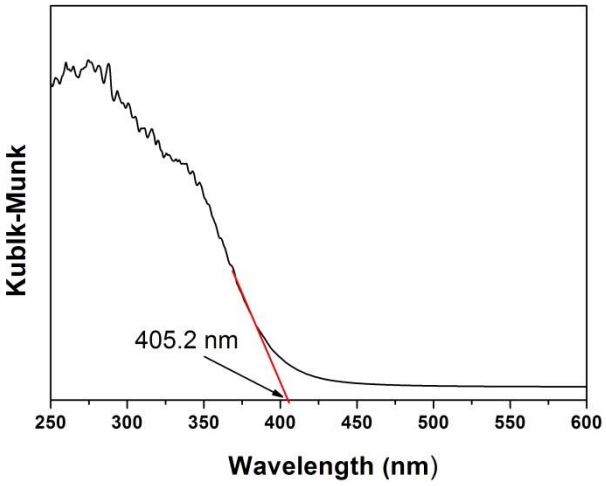

Fig. 5 The UV-Vis diffuse reflectance spectrum of CeO_2 nanowires.

The UV-Vis diffuse reflectance spectrum of the CeO_2 nanowires is shown in Fig. 5. The spectrum exhibits a strong absorption band at the UV region due to the charge-transfer transitions from O 2p to Ce 4f bonds, which can be explained based on the well-known f to f spin-orbit splitting of the Ce 4f state [31]. The absorbing band edge is at 405.2 nm, which meant that the estimated direct band gap energy was 3.06 eV for the CeO_2 nanowires.

3.2 Gas sensing properties

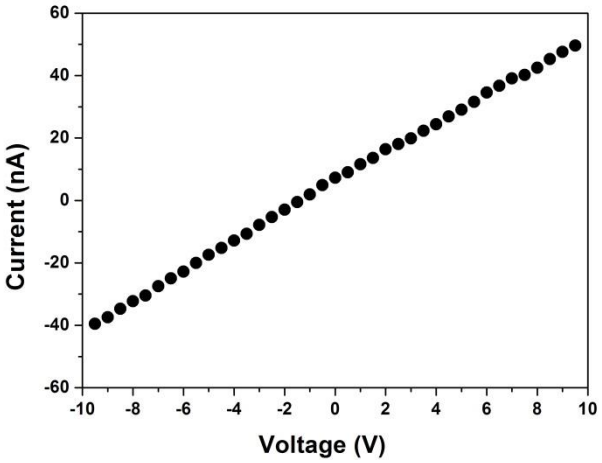

Fig. 6 I-V characteristics between the two electrodes bridged by the CeO_2 nanowires

film at room temperature

Fig. 6 plots a typical current-voltage (I-V) curve between the two electrodes bridged by the CeO_2 nanowires at room temperature. The current increases linearly with the applied bias voltage (from －10 V to 10 V). Such a linear behavior reveals that a good ohmic contact was established between the CeO_2 nanowires and two electrodes. In addition, the I－V curve is non-hysteretic, indicating that the wire to wire connectivity is fairly good. The resistance of the nanowires film calculated from the slope of the curve is 172.0 MOhm.

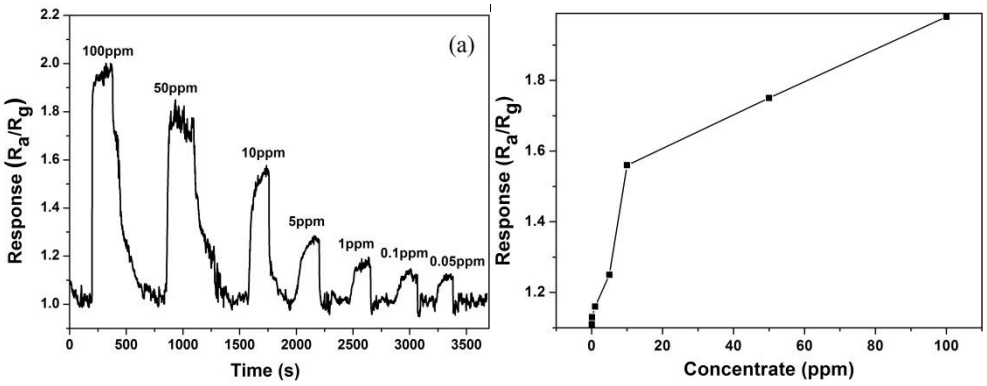

Fig. 7 (a) Dynamic response-recovery curve and (b) response sensitivity of the CeO_2 nanowires based sensor to H_2S gas with different concentrations at room temperature.

Fig. 7a shows the response-recovery curves of the sensor exposed to different concentrations of H_2S gas at room temperature. For all the measurements in the dry air, the gas sensor showed a constant and stable baseline. When the H_2S gas was introduced into the chamber, the resistance of the gas sensor underwent a quick decrease. However, when the chamber was refilled with the dry air, it was also quickly recovered to its original baseline. It is in a good agreement with the sensing

mechanism of n-type semiconductor gas sensor [16]. After several cycles of gas injection and air purging alternatively, a full recovery to the initial readings was achieved, indicating a good reversibility of the gas sensor at room temperature. The response sensitivity of the gas sensor to the H_2S (from 0.05 to 100 ppm) was calculated and the results are shown in Fig. 7b. The response sensitivity increased with the increasing concentration of the H_2S, and it showed a good response to the low concentration ranges of sub-ppm level. The sensor showed a significant response to the concentration as low as 50 ppb with the response value of 1.11, indicating that the gas sensor has a good sensitivity at room temperature.

CeO_2 is an n-type metal oxide semiconductor and its sensing performance is determined by the changes of the resistance which are resulted from the chemical reactions between the testing gases and the oxygen species adsorbed on the surface of the sensor [34,35]. When the CeO_2 nanowires based sensors are exposed to the air, the oxygen molecules are absorbed on the surface of the CeO_2 nanowires. Negatively charged chemisorbed oxygen species are formed by extracting electrons from conduction band of the CeO_2 nanowires which causes a decrease in conductivity of the sensor. Consequently, an electron-depletion layer is formed on the surface [36,37]. The types of absorbed oxygen species are dependent on the working temperature. At room temperature, O_2^- is commonly chemisorbed on the surfaces of the CeO_2 nanowires [38]. The detail reaction at room temperature could be described as follows:

$$O_{2(g)} \rightarrow O_{2(ad)} \quad (4)$$

$$O_{2(ad)} + e^- \rightarrow O^-_{2(ad)} \quad (5)$$

When the sensor is exposed to the H_2S gas, the H_2S molecules are adsorbed onto the surfaces of the CeO_2 nanowires. Because the CeO_2 have strong redox capability, it was in favor of the redox reaction of H_2S gas on the surface of CeO_2[1-3]. They will react with the previously absorbed oxygen species (O_2^-) and generate sulfur oxides and H_2O vapor. The reaction between the H_2S gas and absorbed oxygen species could be expressed using the following equation [38,39]:

$$2H_2S + 3\,O^-_{2(ad)} \leftrightarrow 2H_2O_{(g)} + 2SO_{2(g)} + 3\,e^- \quad (6)$$

During this process, the electrons will be released into the conduction band of the CeO_2 nanowires. As the result, the thickness of the electron-depletion layer is reduced and the resistance of the CeO_2 nanowires decreases as well.

According to the sensing mechanisms of the semiconductors [36-39], the good H_2S sensing performance of the CeO_2 nanowires is related to the following factors. Firstly, the diameter of the crystalline nanowires is less than 12.5 nm, and the surface area of the nanowires is significantly large. Therefore, the size effect is favorite for the good sensing performance of the nanowires. Secondly, the good sensing performance may be attributed to the fact that there are some defects on the surfaces of CeO_2 nanowires (see the Fig. 3c), which could provide the extra reaction sites during the gas sensing.

The response and recovery time were defined as the time to reach 90% of the maximum sensing response upon injecting of testing gas and the time to reach 10% of

the maximum sensing response upon purging with dry air. Fig. 8 shows the response and recovery time of the CeO_2 nanowires based gas sensor at different H_2S gas concentrations. The gas sensor showed a fast response and the recovery time of less than 100 s and 260 s for different concentrations. In addition, at the low concentration below 1 ppm, the response and the recovery time were about 50 s and 20 s, respectively. The fast response and recovery are attributed to the smaller size diameter, larger surface area and more defects on the surface of CeO_2 nanowires, which are all beneficial for the fast absorption and desorption of the H_2S molecules. It should also be mentioned that the response time showed only little variation upon exposed to different concentrations of the H_2S gas. Because the desorption of H_2S molecules became slow at a higher concentration of the H_2S gas, the recovery time increased obviously with increasing the H_2S concentration from 10 to 100 ppm.

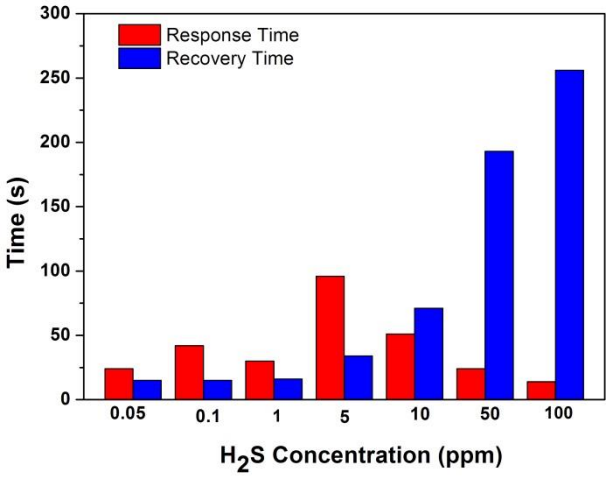

Fig. 8 Response and recovery time of the CeO_2 nanowires based sensor to H_2S gas at room temperature.

Reproducibility of the sensor was demonstrated by successively exposing it to the H_2S gas at a concentration of 100 ppm for 5 cycles at room temperature, and the

results are shown in Fig. 9a. During the repeated gas injection and purging with dry air in the five consecutive sensing cycles, the response-recovery curves of the sensor are almost identical. From the data of the long-term stability shown in Fig. 9b, the largest deviation of the response sensitivity is less than 5% after continuous sensing testing for 20 days, indicating that the sensor possesses an excellent reproducibility and long-term stability for the H_2S detection.

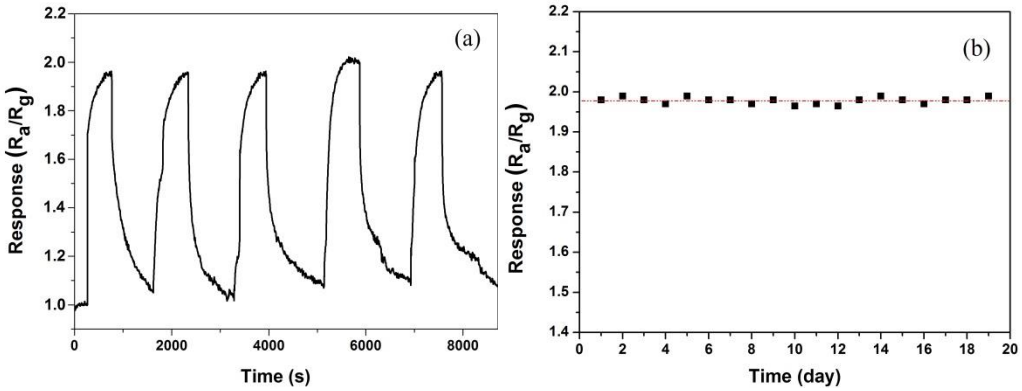

Fig. 9 (a) Response-recovery curve of the gas sensor to 100 ppm H_2S gas for 5 cycles，(b) Long-term stability of the gas sensor to 100 ppm H_2S gas for 20 days at room temperature.

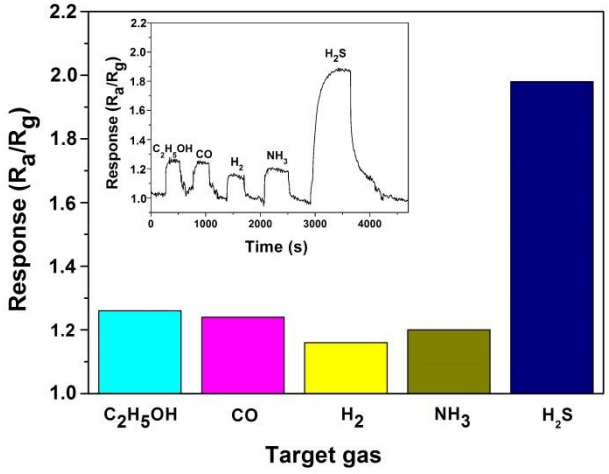

Fig.10 Selectivity histogram of the CeO_2 nanowires based sensor toward difference gases (C_2H_5OH, CO, H_2, NH_3 and H_2S) at the same concentration of 100 ppm

at room temperature (inset indicates the actual measurement curve).

The responses of the gas sensor to several types of the reducing gases (C_2H_5OH, CO, H_2, NH_3 and H_2S) were measured with the same gas concentration of 100 ppm at room temperature. The results are shown in Fig. 10. The inset in the Fig. 10 shows the response curves when the sensor was exposed to the different target gases. Clearly, the sensor displays remarkably higher response to the H_2S gas compared those to the other gases at the same testing conditions. As is shown in Fig. 10, the responses to C_2H_5OH, CO, H_2, NH_3 with the same concentration was 1.25, 1.23, 1.15 and 1.19, respectively. These data, which are far less than that to the H_2S gas at the same concentration of 1.98, suggesting that the sensor has a good selectivity toward H_2S gas.

4. Conclusions

In summary, based on a facile hydrothermal process without using any template or surfactant, the CeO_2 nanowires were successfully synthesized without further heat treatment. The CeO_2 nanowires are uniform with an average diameter of 12.5 nm. The nanowires were single crystalline with a preferred orientation along [111]. At room temperature, the CeO_2 nanowires based on gas sensor showed good sensitivity, rapid response/recovery time, low detection limit, long term stability and good selectivity towards H_2S, indicating that the CeO_2 nanowires prepared by this method can be a promising sensing material for fabrication high-performance H_2S gas sensor.

Acknowledgments

This work was supported by the Joint Fund of the National Natural Science Foundation of China and the China Academy of Engineering Physics (U1330108). Funding support from the UoA and CAPEX from Northumbria University at Newcastle, and Royal academy of Engineering UK-Research Exchange with China and India is also acknowledged.

Reference

[1] F. Yang, J. Graciani, J. Evans, P. Liu, J. Hrbek, J.F. Sanz, J.A. Rodriguez, CO oxidation on inverse CeO(x)/Cu(111) catalysts: high catalytic activity and ceria-promoted dissociation of O_2, J. Am. Chem. Soc. 133 (2011) 3444–3451.

[2] J.F. Li, G.Z. Lu , H.F. Li, Y.Q. Wang, Y. Guo, Y.L. Guo, Facile synthesis of 3D flowerlike CeO_2 microspheres under mild condition with, high catalytic performance for CO oxidation, J. Colloid Interface Sci. 360 (2011) 93–99.

[3] N. Michael, S.C. Parker and G.W. Watson, CeO_2 catalysed conversion of CO, NO_2 and NO from first principles energetic, Phys. Chem. Chem. Phys. 8 (2006) 216–218.

[4] Z.R. Tang, Y.H. Zhang and Y.J. Xu, A facile and high-yield approach to synthesize one-dimensional CeO_2 nanotubes with well-shaped hollow interior as a photocatalyst for degradation of toxic pollutants, RSC Advances 1 (2011) 1772–1777.

[5] Y.C. Zhang, M. Lei, K .Huang, C. Liang, Y.J. Wang, S.S. Ding, R. Zhang, D.Y. Fan, H.J. Yang, Y.G. Wang, A facile route to mono-dispersed CeO_2 nanocubes and their enhanced photocatalytic properties , Mater. Lett. 116 (2014) 46–49.

[6] X.H. Lu, D.Z. Zheng, P. Zhang, C.L. Liang, P. Liu and Y.X. Tong, Facile synthesis of free-standing CeO_2 nanorods for photoelectrochemical applications, Chem. Commun., 46 (2010) 7721–7723.

[7] R. Suresh, V. Ponnuswamy, R. Mariappan, Effect of annealing temperature on the

microstructural, optical and electrical properties of CeO_2 nanoparticles by chemical precipitation method, Appl. Surf. Sci. 273 (2013) 457–464.

[8] L.N. Wang, F.M. Meng, K.K. Li, F. Lu, Characterization and optical properties of pole-like nano-CeO_2 synthesized by a facile hydrothermal method, Appl. Surf. Sci. 286 (2013) 269–274.

[9] J. Zhang, H. Kumagai, K. Yamamura, S. Ohara, S. Takami, A. Morikawa, H. Shinjoh, K.Kaneko, T. Adschiri and A. Suda, Extra-low-temperature oxygen storage capacity of CeO_2 nanocrystals with cubic facets, Nano Lett. 11 (2011) 361–364.

[10] M.J. Li, S.H. Ge, W. Qiao, L. Zhang, Y.L. Zuo, and S.M. Yan, Relationship between the surface chemical states and magnetic properties of CeO_2 nanoparticles, Appl. Phys. Lett. 94 (2009) 152511.

[11] C.A.B. Paula, D.A.A. Santos, J.G.S. Duque, M.A. Macêdo, Structural and magnetic study of Fe-doped CeO_2, Physica B 405 (2010) 1821–1825.

[12] M.S. Anwar , S. Kumar , F. Ahmed , N. Arshi, G.S. Kil , D.W. Park ,J. Chang, B.H. Koo, Hydrothermal synthesis and indication of room temperature ferromagnetism in CeO_2 nanowires, Mater. Lett. 65 (2011) 3098–3101.

[13] S. Maensiri, C. Masingboon, P. Laokul, W. Jareonboon, V. Promarak, P.L. Anderson and S. Seraphin, Egg white synthesis and photoluminescence of platelike clusters of CeO_2 nanoparticles, Cryst. Growth Des. 7 (2007) 950–955.

[14] K. Woan, Y.Y. Tsai, W. Sigmund, Synthesis and characterization of luminescent cerium oxide nanoparticles, Nanomedicine-UK 5 (2010) 233–242.

[15] R.C. Deus, C.R. Foschini, B. Spitova, F. Moura, E. Longo, A.Z. Simoes, Effect of soaking time on the photoluminescence properties of cerium oxide nanoparticles, Ceramics Internationa l40 (2014) 1–9.

[16] L. Liao, H.X. Mai, Q. Yuan, H.B. Lu, J.C. Li, C. Liu, C.H. Yan, Z.X. Shen, T. Yu, Single CeO2 nanowire gas sensor supported with Pt nanocrystals: gas sensitivity, surface bond states, and chemical mechanism, J. Phys. Chem. C 112 (2008) 9061–9065.

[17] N.F. Hamedani, A.R. Mahjoub, A.A. khodadadi, Y. Mortazavi, CeO_2 doped ZnO flower-like

nanostructure sensor selective to ethanol in presence of CO and CH_4, Sens. and Actuators B 169 (2012) 67–73.

[18] C. Chen, C. Liu, Doped ceria powders prepared by spray pyrolysis for gas sensing applications, Ceram. Int. 37 (2011) 2353–2358.

[19] R. Bene, I.V. Perczel, F. ReAti, F.A. Meyer, M. Fleisher, H. Meixner, Chemical reactions in the detection of acetone and NO by a CeO_2 thin, Sens. Actuators B 71 (2000) 36–41.

[20] Y.L. Xuan, J. Hu, K.L. Xu, X.D. Hou, Y. Lv, Development of sensitive carbon disulfide sensor by using its cataluminescence on nanosized-CeO_2, Sens. and Actuators B 136 (2009) 218–223.

[21] X.Q. Fu, C. Wang, H.C. Yu, Y.G. Wang and T.H. Wang, Fast humidity sensors based on CeO_2 Nanowires, Nanotechnology 18 (2007) 776–789.

[22] X.H. Lu, T. Zhai, H.N. Cui, J.Y. Shi, S.L. Xie, Y.Y. Huang, C.L. Liang and Y.X. Tong, Redox cycles promoting photocatalytic hydrogen evolution of CeO_2 nanorods, J. Mater. Chem. 21 (2011) 5569–5572.

[23] H.J. Tang, H.Y. Sun, D.R. Chen, X.L. Jiao, Fabrication of Pt/CeO_2 nanofibers for use in water–gas shift reaction, Mater. Lett. 77 (2012) 7–9.

[24] R.U. Yang, L. Guo, Synthesis of cubic fluorite CeO2 nanowires, J. Mater. Sci. 40 (2005) 1305–1307.

[25] G.Z. Chen, C.X. Xu, X.Y. Song, W. Zhao, Y.Ding and S.X. Sun, Interface reaction route to two different kinds of CeO_2 nanotubes, Inorg. Chem. 47 (2008) 723–728.

[26] A.D. Liyanage, S.D. Perera, K.Tan, Y. Chabal and K.J.B. Jr, Synthesis, characterization, and photocatalytic activity of Y‑doped CeO_2 nanorods, ACS Catal. 4 (2014) 577–584.

[27] T.M. Liu, C.L. Chen, W.W. Guo, R. Sun, S.H. Lv, M. Saito, S. Tsukimoto, Z.C. Wang, Synthesis and characterization of CeO_2 nano-rods Yong Chen, Ceram. Int. 39 (2013) 6607–6610.

[28] X.W. Liu, K.B. Zhou, L. Wang, B.Y. Wang and Y.D. Li, Oxygen vacancy clusters promoting reducibility and activity of ceria nanorods, J. Am. Chem. Soc. 131 (2009) 3140–3141.

[29] R.B. Yu, L. Yan, P. Zheng, J. Chen and X.R. Xing, Controlled synthesis of CeO_2 flower-like and well-aligned nanorod hierarchical architectures by a phosphate-assisted hydrothermal route, J. Phys. Chem. C 112 (2008) 19896–19900.

[30] A. Vantomme, Z.Y. Yuan, G.H. Du and B.L. Su, Surfactant-assisted large-scale preparation of crystalline CeO_2 nanorods，Langmuir 21 (2005) 1132–1135.

[31] D.S. Zhang, H.X. Fu, L.Y. Shi, C.S. Pan, Q. Li, Y.L. Chu and W.J. Yu, Synthesis of CeO_2 nanorods via ultrasonication assisted by polyethylene glycol, Inorg. Chem. 46 (2007) 2446–2451.

[32] F. Larachi, J. Pierre, A. Adnot, A. Bernis, Ce3d XPS study of composite CexMn1-xO2-wet oxidation catalysts, Appl. Surf. Sci. 195 (2002) 236–250.

[33] A.Q. Wang, P. Punchaipetch, R.M. Wallace, T.D. Golden, X-ray photoelectron spectroscopy study of electrodeposited nanostructured CeO_2 films, J. Vac. Sci. Technol. B 21 (2003) 1169–1175.

[34] J. Kim, K. Yong, Mechanism study of ZnO nanorod-bundle sensors for H_2S gas sensing, J. Phys. Chem. C. 115 (2011) 7218–7224.

[35] Z. Wen, L.P. Zhu, Y.G. Li, Z.Y. Zhang, Z.Z. Ye, Mesoporous Co_3O_4 nanoneedle arrays for high-performance gas sensor, Sens. Actuators. B. 203 (2014) 873–879.

[36] Z.J. Li, Y.W. Huang, S.C Zhang, W.M Chen, Z. Kuang, D.Y. Ao, W. Liu, Y.Q. Fu, A fast response & recovery H_2S gas sensor based on α-Fe_2O_3 nanoparticles with ppb level detection limit, J. Hazard. Mater. 300 (2015) 167–174.

[37] S.J. Chang, T.J. Hsueh, I.C. Chen, B.R. Huang, Highly sensitive ZnO nanowire CO sensors with the adsorption of Au nanoparticles, Nanotechnology. 19 (2008) 2039–2042.

[38] Y.W. Huang, W.M. Chen, S.C. Zhang, Z. Kuang, D.Y. Ao, N.R. Alkurd, W.L. Zhou, W. Liu, W.Z. Shen, Z.J. Li, A high performance hydrogen sulfide gas sensor based on porous α-Fe_2O_3operates at room-temperature, Appl. Surf. Sci. 351 (2015) 1025–1033.

[39] K. Yao, D. Caruntu, Z.M. Zeng, J.J. Chen, C.J. O'Connor, W.L. Zhou, parts per billion-level H2S detection at room temperature based on self-assembled In_2O_3 nanoparticles, J. Phys. Chem. C

113 (2009) 14812–14817.